Direct Incorporation of Magnetic Constituents within Ordered Mesoporous Carbon–Silica Nanocomposites for Highly Efficient Electromagnetic Wave Absorbers

ARTICLE *in* THE JOURNAL OF PHYSICAL CHEMISTRY C · APRIL 2010

Impact Factor: 4.77 · DOI: 10.1021/jp911030n

Direct Incorporation of Magnetic Constituents within Ordered Mesoporous Carbon−Silica Nanocomposites for Highly Efficient Electromagnetic Wave Absorbers

Jianhua Zhou, Jianping He,* Guoxian Li, Tao Wang, Dun Sun, Xiaochun Ding, Jianqing Zhao, and Shichao Wu

College of Material Science and Technology, Nanjing University of Aeronautics and Astronautics, Nanjing 210016, P. R. China

Received: November 20, 2009; Revised Manuscript Received: March 22, 2010

Low-density ordered mesoporous carbon−silica nanocomposites with different Fe contents have been prepared by a facile solvent-evaporation-induced self-assembly approach. Magnetic metal nanocrystallines are highly dispersed in the composites due to *in situ* carbothermal reduction. The optimal reflection loss calculated from the measured permittivity and permeability is −34.4 dB at 13.1 GHz. Moreover, the electromagnetic wave absorption less than −10 dB is found to exceed 5.0 GHz for an absorber thickness of 2 mm. The microwave enhancement absorption of the mesoporous C−SiO_2−Fe nanocomposites is contributed to the better match between dielectric loss and magnetic loss, which originates from the high absorption by the incorporation of magnetic species as well as the multiple reflections by the ordered mesoporous structure. The mesoporous C−SiO_2−Fe nanocomposites also exhibit a lower infrared emissivity in the wavelength from 8 to 14 μm than that of Fe-free powder.

Introduction

With the explosive development of information technology using the electromagnetic wave of gigahertz (GHz) range, serious electromagnetic interference problems have emerged. The electromagnetic interference pollution can cause disturbances on the equipment and systems for medical, industrial, commercial, and military applications. Microwave radiation is also potentially harmful to biological systems which are continuously exposed to microwave for a considerable period of time. Electromagnetic interference shielding or microwave absorbing materials have been used to attenuate those unwanted electromagnetic energies, which is an important issue to be considered for both civil and military purposes. Therefore, considerable attention has been devoted to the effective electromagnetic wave absorbing materials with lightweight and strong absorption over a broad frequency spectrum.[1−4]

In particular, carbon materials, such as carbon black,[5] graphite flakes,[6] carbon fiber,[7] and carbon nanotubes,[8] have long been explored as possible electromagnetic shielding and microwave absorbing materials, especially in the case of lightweight and harsh environment. The reflection loss of multiwalled carbon nanotube/SiO_2 nanocomposite was below −10 dB in the frequency range 8.2−12.4 GHz even at a high temperature of 600 °C.[9] However, the pure carbon materials contribute to microwave energy absorption mostly because of their dielectric loss. The dielectric permittivity and magnetic permeability are out of balance; in this way, most of the microwave radiation is reflected, rather than absorbed. An impedance-matching strategy has been devised for carbon materials, such as incorporating with magnetic constituents or decreasing dielectric permittivity.

The lack of magnetic loss of carbon materials in the microwave absorbing process is a key factor pointed out as a problem for its use as a microwave absorbing material.[10,11] This can be achieved by dispersing magnetic particles into a carbon matrix. The amorphous carbon or graphite prevents the intrinsical aggregation of magnetic particles and reduces the magnetic coupling between individual nanoparticles.[12,13] The nanocomposites, with magnetic compounds encapsulated in the pores or attached on the outer surface of carbon nanotubes,[14,15] are found to have complementary advantages. It is favorable to strong absorption in a wide frequency range. A magnetic layer can be coated onto the carbon nanotubes by an electroless deposition method.[16] It contributes the soft magnetic characteristics to carbon nanotubes and improves the microwave absorption property. However, the dispersion of carbon nanotubes in the polymer matrix is still a concerning problem.

On the other hand, introducing vacancies or pores in the microwave absorbing materials is effective to reduce the complex relative dielectric permittivity as well as the density of the powders. Porous iron powders have been prepared by burning out the composites of activated carbon impregnating with concentrated metal nitrate solutions. The prepared materials with a broad pore size distribution could largely reduce the complex relative dielectric permittivity without decreasing the complex relative magnetic permeability.[17] They could match well when the pores were introduced. Interestingly, the porous Fe_3O_4/SnO_2 core−shell nanorods exhibit dual-frequency absorption characteristics, as the absorber thickness is 4 mm, which is attributed to effective complementarities between the dielectric loss and the magnetic loss.[18] On the basis of the recent success and popularity of ordered mesoporous carbons with designed pore architecture,[19] it becomes increasingly attractive to consider the preparation of microwave absorbers taking advantage of their unique properties and further functionalization. An elaborate nanostructure comprised of hexagonally ordered mesoporous carbon CMK-3 and fused silica presented excellent electromagnetic interference shielding efficiency, and the contribution of microwave absorption was found to be much higher than that of the reflection. The mesostructure can reflect and scatter the incident microwaves many times. Notably, the electromagnetic energy could be completely absorbed because the microwave

* To whom correspondence should be addressed. Phone: +86 025 52112900. Fax: +86 025 52112626. E-mail: jianph@nuaa.edu.cn.

10.1021/jp911030n
Published on Web 04/12/2010

cannot escape from the confined space.[20] In addition, the chemical composition of the mesoporous framework can be easily modulated and thus yield hybrid nanocomposites with controllable constituent ratio.[21] By simply adding inorganic salt to the reaction mixture through self-assembly of resol and Pluronic F127, highly ordered metal-containing mesoporous carbons have been synthesized via a solvent-evaporation-induced self-assembly (EISA) approach.[22−24] Metal ions were reduced to metallic nanoparticles during the carbonization and then highly dispersed in the carbon matrix, while the ordered mesostructure remained well. With ferric citrate as a metal precursor, the interaction between metal complex and resol was enhanced. An ordered mesostructure with a homogeneous dispersion of maghemite can be obtained after pyrolysis at 600 °C.[25] Therefore, the incorporation of magnetic constituents and the creation of vacancies can be achieved simultaneously.

In our previous studies,[26] we have found that ordered mesoporous C−Al_2O_3 composites show excellent infrared camouflaging effectiveness and could be used as a promising lightweight coating in civil and military fields. Here, the purpose of this study was to investigate the electromagnetic and microwave absorption properties of the designed mesoporous nanocomposites. Carbon−silica nanocomposites with highly dispersed Fe species were prepared by a simple EISA route with triblock copolymer F127 as a structure-directing agent, ferric chloride and tetraethyl orthosilicate (TEOS) as inorganic precursors, and furfuryl alcohol as a carbon precursor. It was found that the combination of ordered mesoporous structure and the incorporation of magnetic species contributed to the enhanced microwave absorption in a wide band. It can be further expanded to infrared band at a wavelength of 8−14 μm.

Experimental Section

Materials. Poly(propylene oxide)-block-poly(ethylene oxide)-block-poly(propylene oxide) triblock copolymer Pluronic F127 (M_w = 12 600, $PEO_{106}PPO_{70}PEO_{106}$) was purchased from Sigma-Aldrich. TEOS, furfuryl alcohol, $FeCl_3 \cdot 6H_2O$, ethanol, and dimethylbenzene were purchased from Sinopharm Chemical Reagent Co. Ltd., China. EPDM (ethylene propylene diene monomer) was provided by Jiangsu Jiangyin Forwell Trade Co. Ltd., China. All chemicals were used as received without any further purification. Millipore water was used in all experiments.

Preparation of Mesoporous Nanocomposites. In a typical synthesis, F127 (1.0 g) was poured into ethanol (10.0 g) with vigorous stirring to obtain a clear solution. With ferric chloride as a precursor, Fe was then introduced under stirring at 40 °C for another 1 h. To this solution, TEOS (1.04 g) and furfuryl alcohol (0.5 mL) were added in succession. After stirring for 2 h, a homogeneous solution was obtained. The solution was transferred into dishes to evaporate ethanol under room temperature and then thermopolymerized in an oven at 80 °C for 24 h. The carbonization was carried out under a N_2 atmosphere using always a heating rate of 1 °C·min^{-1}. The resulting nanocomposites are denoted as CS-*x*Fe-*y*, where *x* and *y* represent the content (mmol) of $FeCl_3$ added initially and the final temperature (°C) of carbonization, respectively. For comparison, the pure carbon−silica nanocomposite CS-700 was prepared by the same process without metal chloride.

Characterization. The samples were characterized by field emission scanning electron microscopy (FE-SEM, Hitachi S-4800), transmission electron microscopy (TEM, FEI Technai G^2 and JEM 2100), and X-ray powder diffraction (XRD, Bruker D8 Advance diffractometer with Cu Kα source). Nitrogen adsorption−desorption isotherms were measured at 77 K using a Micromeritics ASAP 2010 system. Surface areas of the samples were calculated using the BET (Bruauer−Emmett−Teller) equation, while the pore size distributions were determined by the BJH (Barret−Hoyner−Halenda) method using the adsorption branch.

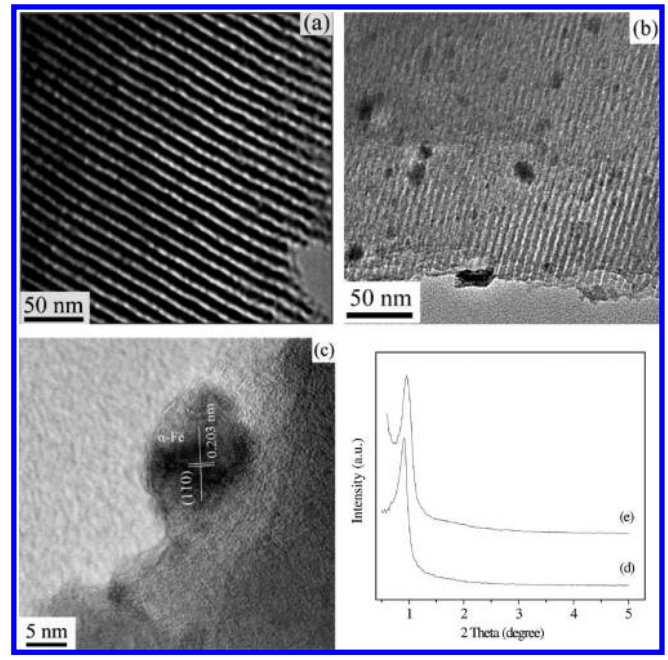

Figure 1. TEM images from (a) CS-700 and (b) CS-Fe-700. High-resolution TEM image of (c) an iron nanoparticle of CS-Fe-700. Small-angle XRD profiles of (d) CS-700 and (e) CS-Fe-700.

Microwave Measurement. The prepared powder was dispersed in commercial epoxy resin which was used as a binder matrix (the weight ratio of the prepared powder was about 40%), and then, the mixture was pressed into a toroid with an outer diameter of 7.0 mm, inner diameter of 3.04 mm, and height of about 3.0 mm. The complex relative dielectric permittivity and magnetic permeability were obtained by measuring the S_{11} and S_{21} parameters over 0.5−18 GHz using a vector network analyzer (Agilent E8363A). To reduce the errors, all values were obtained by averaging over the data measured from three different toroids of each sample.

Infrared Emissivity Measurement. Aluminum sheet, previously degreased in diluted NaOH at 50 °C and then chemically polished in diluted HNO_3, was used as the substrate for the coatings. EPDM dissolved in dimethylbenzene was used as the adhesive. The prepared powder was used as the filling, and its weight ratio was set as 30% in the coating. The coating thickness could be adjusted at 30 and 40 μm by the wire-wound rod coater. The infrared emissivity value at a wavelength of 8−14 μm was measured by using an IR-2 Infrared Emissometer (Shanghai Institute of Technological Physics of the Chinese Academy of Sciences). All values were obtained by averaging over the data measured from 10 different regions of each coating.

Results and Discussion

A controllable synthesis of highly ordered mesoporous carbon−silica nanocomposites with magnetic constituents can be realized by using an EISA approach. Figure 1 reveals the mesoporous structure by TEM and small-angle XRD. It can be clearly seen that mesoporous channels are highly arranged and parallel to each other in the [110] direction, indicating a large region of ordered mesopores in CS-700 (Figure 1a). As shown in Figure 1b, a relatively poor-resolved channel with rough pore

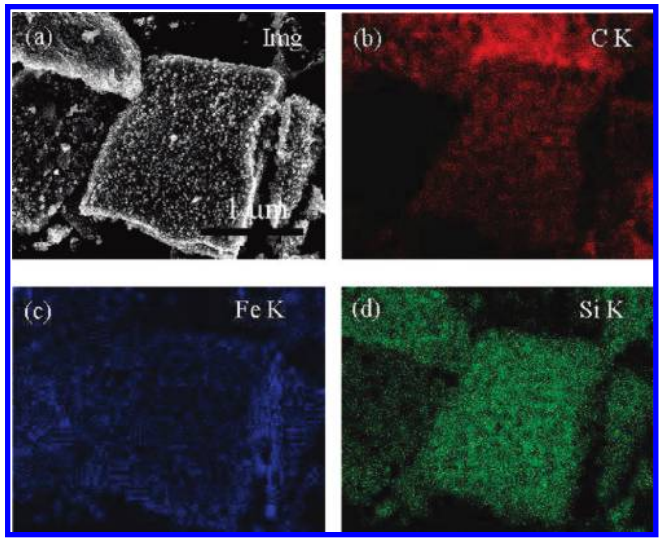

Figure 2. (a) FE-SEM image of the nanocomposite CS-Fe-700. (b−d) Elemental maps of C, Fe, and Si in CS-Fe-700, respectively.

surface is observed for CS-Fe-700, although the uniform and regular mesostructure remained. Iron nanoparticles are dispersed in the amorphous carbon−silica frameworks and estimated to be 10 nm in diameter. A high-resolution TEM image (Figure 1c) shows that the measured interlayer spacing is 0.203 nm, which is consistent with the crystal lattice plane (110) of α-Fe.[27] Supporting the TEM results, the small-angle XRD pattern (Figure 1d) of CS-700 shows a well-resolved diffraction peak around a 2θ angle of 0.9°, which belongs to typical 2D hexagonal mesostructure.[28] The diffraction slightly shifts to high angle (Figure 1e) for CS-Fe-700, suggesting that the mesopore is reduced. This is further confirmed by the nitrogen adsorption−desorption isotherms. During the carbonization process, the metal constituents could be easily reduced by carbon at 700 °C and endow a magnetic property to the carbon−silica nanocomposites.[24,29] The wide-angle XRD patterns show that the peaks of α-Fe and Fe_3C exist in CS-Fe-700 (see the Supporting Information, Figure S1). The metal species are highly dispersed in the frameworks during the self-assembly of the mesostructures, and a large number of metal nuclei could be produced in the amorphous carbon−silica matrix during the pyrolysis. However, these metal nanocrystallines could thrust into the channels and cause partial block of the mesopores.[30]

The fine dispersion of carbon, iron, and silicon is confirmed by element mapping in energy dispersive X-ray spectroscopy measurements installed in the FE-SEM system, as shown in Figure 2. Through a simple triconstituent coassembly process, an interpenetrating mesostructured framework with silica as a reinforcing steel bar and carbon as a concrete is easily obtained.[21] This strategy offers the possibility of preparing an ordered mesostructure with a homogeneous framework of other metal species having catalytic or magnetic properties.[22,25,31] Metal chloride would act as a catalyst for the hydrolysis of TEOS, and the resulting silica can reinforce the mesostructured framework. Meanwhile, polyfurfuryl alcohol is formed in this acidic environment. Under a controlled reaction rate, the inorganic and organic species can easily be assembled into a highly ordered mesostructure by the amphiphilic surfactant micelles. Therefore, a uniform dispersion of C, Fe, and Si elements is observed.

Figure 3 shows N_2 sorption isotherms and pore size distributions of the carbon−silica nanocomposites with different Fe contents. All of the nanocomposites with metal constituents exhibit representative type IV isotherms with H_2 type hysteresis loops. The pure carbon−silica powder possesses a marked difference in the relative higher pressure region of strong N_2 adsorption, indicating a larger pore size. The surface areas, pore volumes, and maximum pore sizes are given in Table 1. Indeed, a narrow pore size distribution centered at 7.7 nm is observed for CS-700. With the incorporation of Fe, the pores become smaller, about 4 nm. The BET surface area and pore volume of the Fe-containing sample with a low iron loading (CS-Fe-700) are as high as 499 $m^2 \cdot g^{-1}$ and 0.42 $cm^3 \cdot g^{-1}$. Gradual decrease of those values is found with increasing iron content (Table 1), related to a poor mesostructure.[25] The high porosity in this mesostructure would decrease the bulk density of the prepared powder undoubtedly, making it possible to design a lighter and thinner electromagnetic wave absorber.

The complex permittivity and permeability were measured by the transmission/reflection coaxial line method.[32,33] The real part (ε') and imaginary part (ε'') of the complex relative permittivity ($\varepsilon_r = \varepsilon' - j\varepsilon''$) represent the energy storage and dissipation capability, respectively. Parts a and b of Figure 4 show ε' and ε'' of the prepared powder/resin composites in the frequency range 0.5−18 GHz. The ε' value of iron-free carbon−silica powder (CS-700) decreases from 12.6 to 6.3, while the ε'' value has a slight increase. Thus, the present of carbon−silica will dominate the dielectric loss.[34] When Fe is introduced in the nanocomposites, but just heat-treated at 500 °C, the ε' and ε'' values of CS-Fe-500 are almost constant with nearly no variation throughout the whole frequency range, and the values are relatively low ($\varepsilon' \approx 3.1$, $\varepsilon'' \approx 0.15$), indicating very poor dielectric loss. As the pyrolysis temperature increases,

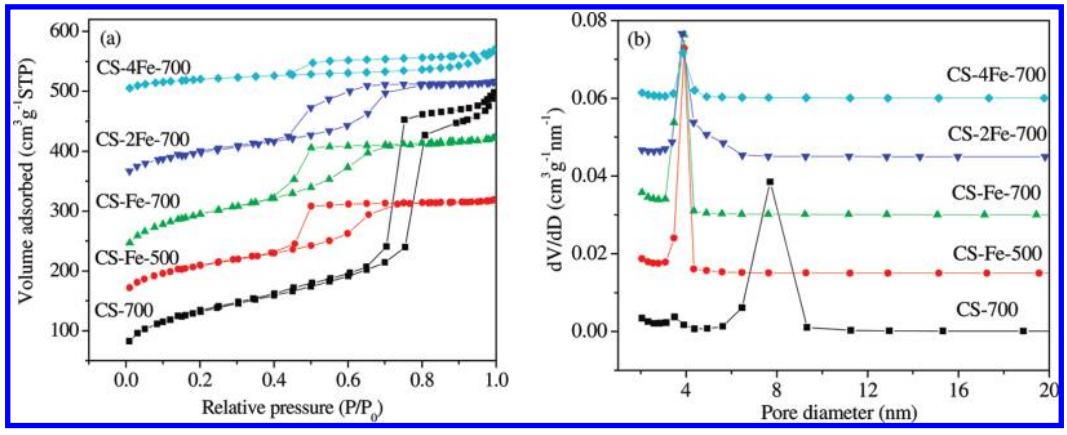

Figure 3. N_2 adsorption−desorption isotherms (a) and the BJH pore diameter distribution curve (b) of the nanocomposites.

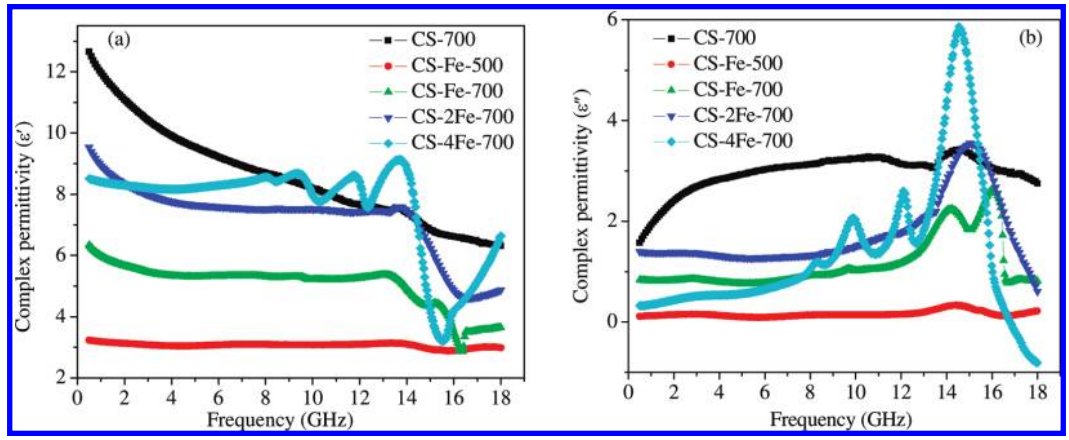

Figure 4. Real (a) and imaginary (b) parts of the complex relative permittivity of the nanocomposites in the frequency range 0.5−18 GHz.

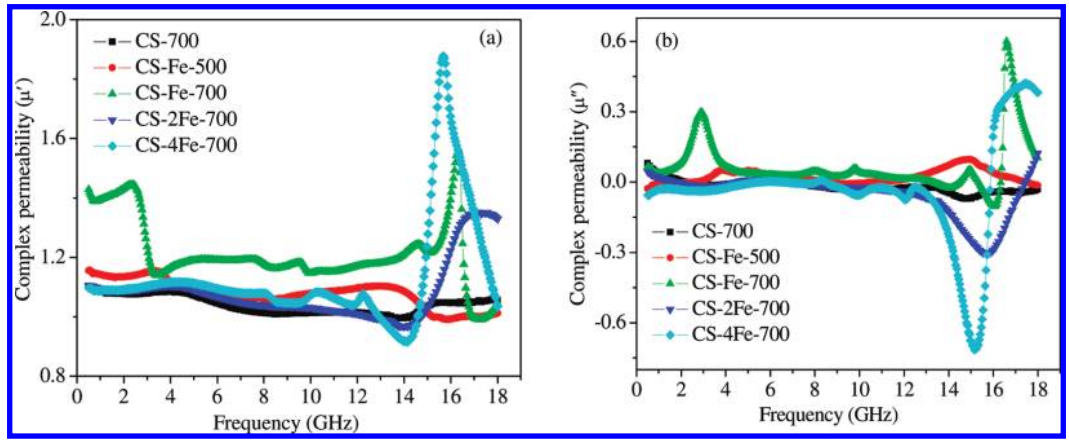

Figure 5. Real (a) and imaginary (b) parts of the complex relative permeability of the nanocomposites in the frequency range 0.5−18 GHz.

TABLE 1: Porous Characteristics Data for the Nanocomposites

sample	BET surface area ($m^2 \cdot g^{-1}$)	total pore volume ($cm^3 \cdot g^{-1}$)	micropore volume ($cm^3 \cdot g^{-1}$)	most probable pore diameter (nm)
CS-700	460	0.77	0.04	7.7
CS-Fe-500	376	0.34	0.04	3.9
CS-Fe-700	499	0.42	0.06	3.9
CS-2Fe-700	336	0.34	0.05	3.8
CS-4Fe-700	233	0.18	0.06	3.8

the complex permittivity becomes higher than that of CS-Fe-500 but has the character of a knee at 13 GHz on the curve. With the greater amount of Fe, the curve shape is similar to that of CS-Fe-700, only with larger permittivity values. However, the values of the complex relative permittivity are under those observed for the pure carbon−silica nanocomposites almost in the whole range 0.5−18 GHz. This is of great benefit in balancing permeability and permittivity, thus decreasing the difficulty of impedance matching for the microwave absorber. It is also noteworthy that there is a resonance peak around the frequency range 14−16 GHz in the curves of the imaginary part ε'' (Figure 4b), especially for the Fe-containing samples calcined at 700 °C. As mentioned above, the mesopores in the nanocomposites are robust and interconnected, and incident electromagnetic microwaves could take place in energy dissipation many times, in the form of reflection and scattering confined within the hexagonally ordered nanostructure.[17,18,20] It is reasonable to say that the mesoporous framework endows the resonance loss. Furthermore, the architecture with magnetic particles embedded into a carbon−silica matrix would provide additional interfaces around the particles, and the interfacial polarization associated with relaxation can give rise to dielectric loss in high frequency ranges as well.[35]

The real part (μ') and imaginary part (μ'') of the complex relative permeability ($\mu_r = \mu' - j\mu''$) versus frequency for the samples is shown in parts a and b of Figure 5, respectively. Without a magnetic element, the pure carbon−silica powder exhibits an almost constant complex relative magnetic permeability. Due to the amorphous iron species formed at 500 °C heat treatment (Figure S1, Supporting Information), the permeability values of CS-Fe-500 increase slightly compared with those of iron-free powder. At the elevated temperature of 700 °C, magnetic metal nanocrystallines occur in the composites as a result of carbothermal reduction. A resonance peak around 3 GHz appears for CS-Fe-700. The ferromagnetic resonance frequency correlates to the effective anisotropy field including demagnetizing and anisotropy fields. However, the natural resonance frequency for bulk α-Fe is only several megahertz,[36] indicating that there is a remarkable increase in the anisotropy energy for CS-Fe-700. Magnetic nanoparticles are highly dispersed in the carbon−silica matrix, and the regular mesopore channels may also act as an isolation strip for the cutoff of the coupling interactions between the neighboring magnetic components. This nanocomposite with isolated magnetic particles possesses high surface area and large porosity, which was shown in Table 1; thus, its surface anisotropy energy would be

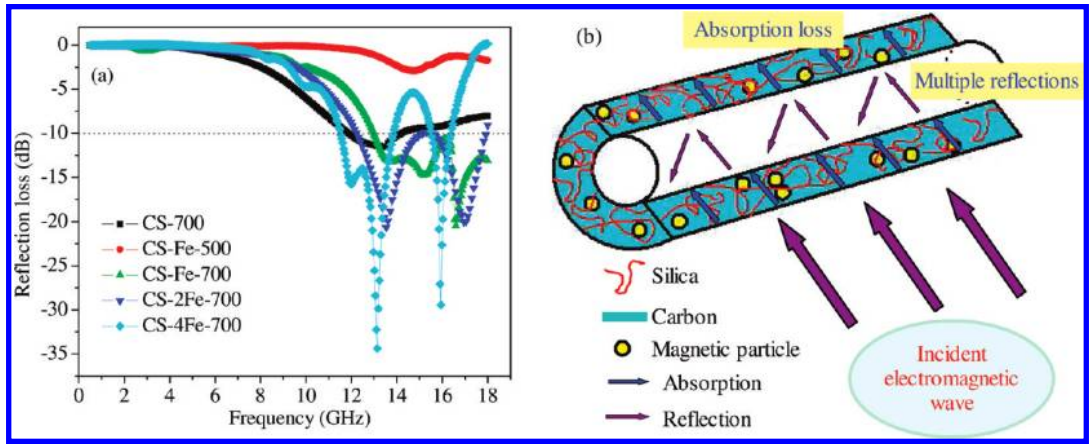

Figure 6. (a) Reflection loss for the nanocomposites, with an absorber thickness of 2 mm in the frequency range 0.5−18 GHz. In measurement, a 40 wt % sample and 60 wt % epoxy resin were used. (b) A schematic representation for the possible dissipation route of electromagnetic wave in the ordered mesoporous structure.

remarkably increased.[37] In addition, the unique mesostructure gives rise to a demagnetizing effect,[38] which leads to an increase of the effective anisotropy field and a shift to a higher frequency of the resonance peak.

Interestingly, it is found that the μ'' values are negative in 14−16 GHz for these Fe-containing samples, and the minimum value is up to −0.71. Moreover, this trough is corresponding to the resonance peak of the imaginary permittivity. This phenomenon is also found in some studies for various nanostructures. In one case, a negative μ'' value is considered to be the magnetic energy going out of the absorber, comparing that a positive one means the incident electromagnetic energy being absorbed by the absorber. Shi et al.[39] proposed an equivalent circuit model for the hollow Co nanochains. The inverse change trend of permeability and permittivity is attributed to the phase lag between capacitance and inductance. As the permeability and permittivity are coupled on the basis of the Maxwell equations, the magnetic energy can be produced by the motion of charges and induced into dissipative current. Then, it is radiated out from the absorber.[18,40,41] In the other case, Chiu et al.[42] pointed out that the negative permeability is meaningless in physics but indicated these materials with negative permeability and/or permittivity may have potential as left-handed materials. In our work, an obvious coupling is found in the imaginary parts of permittivity and permeability. It is reasonable that the electric property of the Fe-containing nanocomposites should take responsibility for the phenomenon of a maximum ε'' and a minimum μ'' at the same frequencies, especially at the elevated temperature of 700 °C. The formation of numerous conductive networks at 700 °C increases the electrical conductivity and simultaneously induces a magnetic field. As the ε'' value is in proportion to electrical conductivity, it contributes to the dielectric resonance peak. The induced magnetic energy is then radiated along the conductive networks, with a change of incident wavelength or a conversion to other forms of energy. As discussed above, the mesopores provide the repeated electromagnetic energy dissipation and the metal components contribute the complementary magnetic loss. Therefore, it is in a more favorable position to achieve the balance between dielectric loss and magnetic loss, suggesting that the ordered mesoporous carbon−silica nanocomposites with Fe species have excellent microwave absorption properties.

The possibility of using the mesoporous nanocomposites for microwave absorbing was explored. On the basis of the previously measured electromagnetic parameters (Figures 4 and 5), reflection loss of powder−resin composites can be obtained by calculation and simulation. The electromagnetic wave travels through free space, which has an impedance of Z_0 (eq 1).

$$Z_0 = \sqrt{\frac{\mu_0}{\varepsilon_0}} \tag{1}$$

where μ_0 and ε_0 are the complex relative permeability and permittivity of free space. When the microwave then propagates on a medium surface, the input impedance Z_{in} can be described using eq 2.[43]

$$Z_{in} = Z_0\sqrt{\frac{\mu_r}{\varepsilon_r}}\tanh\left[j\frac{2\pi fd}{c}\sqrt{\mu_r\varepsilon_r}\right] \tag{2}$$

where μ_r and ε_r are the complex relative magnetic permeability and dielectric permittivity of the composite medium, respectively, c is the velocity of electromagnetic waves in free space, f is the frequency of microwaves, and d is the thickness of an absorber. According to transmission line theory, for a single-layer absorbing material backed by a perfect conductor, the reflection loss of normal incident electromagnetic wave on the absorber surface, R (dB), is given by the following equation:[44]

$$R = 20\log\left|\frac{Z_{in} - Z_0}{Z_{in} + Z_0}\right| \tag{3}$$

The calculated reflection loss as a function of frequency for these samples is shown in Figure 6a, where d is assumed as 2.0 mm. The pure carbon−silica powder shows a maximum reflection loss of −11.6 dB at 13.4 GHz, while CS-Fe-500 shows a maximum reflection loss of only −2.9 dB at 14.7 GHz. There is no absorption range under −10 dB for CS-Fe-500, and the effective absorption bandwidth which is lower than −10 dB is only 2.3 GHz for CS-700. For the Fe-containing samples calcined at 700 °C, they exhibit dual-frequency absorption characteristics. The relative weak absorption peaks are about −14.7, −20.0, and −29.5 dB, and the strongest peaks could reach −20.5, −20.6, and −34.4 dB with the increasing Fe content. Moreover, the bandwidths lower than −10 dB are 5.0, 5.1, and 3.2 GHz, respectively, as the layer thickness is 2 mm. For the dielectric microwave absorber, it is highly efficient for incorporating a magnetic constituent to enhance complex permeability. Since the complex permittivity of carbon−silica powder is relatively large, its dielectric loss and magnetic loss are out of balance, which induces the poor microwave absorp-

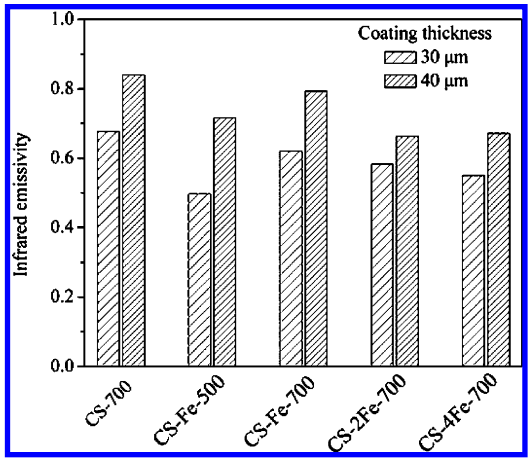

Figure 7. Average infrared emissivity at 8−14 μm of the coatings using EPDM as an adhesive.

tion, at worst, exhibiting a thick matching thickness and narrow absorbing bandwidth.[45] With addition of Fe species and under a proper calcination temperature of 700 °C, the mixed absorbers generally exhibit enhanced absorbing characteristics with wider effective bandwidth and thinner matching thickness. The electromagnetic wave can hardly be reflected on the absorber surface because of a better match between dielectric loss and magnetic loss (Figure 6b), which originates from the combination of dielectric carbon−silica and metallic magnet Fe species. Furthermore, the incident electromagnetic microwaves are confined within the mesostructure of absorbers and multiple reflections induce the energy dissipation occurring in many different sites (Figure 6b). This allows a sufficient absorption within the robust mesostructure. The reflection loss and the effective bandwidth under −10 dB of the Fe-containing samples calcined at 700 °C are better than those of Fe-filled carbon nanotubes,[8,15,16] when the thickness of the composite is 2 mm.

We also confirmed the multifunctional camouflaging ability in the thermal infrared region (8−14 μm) of the prepared powder/EPDM coatings. According to Kirchhoff's law, the emissivity is equal to the absorptivity when the material is opaque for the infrared light. Thus, the high reflection and low absorption of a coating lead to a low emissivity and a better camouflage capability in the infrared wave-band. However, this will emerge in the radar detection. It is necessary to design a material with compatible camouflage capability for radar and infrared wave-band.[46] The histogram for infrared emissivity is given in Figure 7. The pure carbon−silica has high emissivity values of 0.677 and 0.839 corresponding to a coating thickness of about 30 and 40 μm, respectively. Although the emissivity of CS-Fe-500 reaches a minimum value of 0.498, it is clearly seen that CS-2Fe-700 and CS-4Fe-700 display a super performance in both microwave absorbing and infrared camouflaging. The mesostructure with Fe brings multiple reflections for infrared photons. Therefore, the decrease in the emissivity value is attributed to the characteristics of the high porosity in mesostructured nanocomposites.

Conclusions

Highly ordered mesoporous C−SiO_2−Fe nanocomposites have been prepared by a simple EISA method, followed by carbonization. Fe species are dispersed homogeneously in the framework and endow the mesoporous nanocomposites with magnetic property. For dielectric loss, the incorporation of Fe and the mesoporous framework contribute to a dielectric resonance peak in the frequency range 14−16 GHz. In addition, the nanocomposite with isolated magnetic particles possesses high surface area and large porosity, which leads to the shift to higher frequency of the magnetic resonance peak. The Fe-containing nanocomposites exhibited dual-frequency absorption characteristics and the bandwidth lower than −10 dB is as large as 5.1 GHz when the layer thickness is 2 mm. The infrared emissivity values of CS-2Fe-700 and CS-4Fe-700 can be reduced less than 0.6. This material is promising as a light-weight, hard corrosion, and wide-frequency multifunctional camouflage coating. Additionally, our studies also indicate the feasibility of mesoporous nanocomposites coupled to magnetic constituents for the applications in biomedicine, magnetism, catalysis, adsorption, and separation.

Acknowledgment. This work was supported by Natural Science Foundation (50871053) and Aeronautical Science Foundation of China (2007ZF52061).

Supporting Information Available: Wide-angle XRD patterns. This material is available free of charge via the Internet at http://pubs.acs.org.

References and Notes

(1) Che, R. C.; Peng, L. M.; Duan, X. F.; Chen, Q.; Liang, X. L. *Adv. Mater.* **2004**, *16*, 401.
(2) Thomassin, J. M.; Lou, X. D.; Pagnoulle, C.; Saib, A.; Bednarz, L.; Huynen, I.; Jérôme, R.; Detrembleur, C. *J. Phys. Chem. C* **2007**, *111*, 11186.
(3) An, Z. G.; Pan, S. L.; Zhang, J. J. *J. Phys. Chem. C* **2009**, *113*, 2715.
(4) Xu, P.; Han, X. J.; Jiang, J. J.; Wang, X. H.; Li, X. D.; Wen, A. H. *J. Phys. Chem. C* **2007**, *111*, 12603.
(5) Annadurai, P.; Mallick, A. K.; Tripathy, D. K. *J. Appl. Polym. Sci.* **2002**, *83*, 145.
(6) Fan, Y. Z.; Yang, H. B.; Li, M. H.; Zou, G. T. *Mater. Chem. Phys.* **2009**, *115*, 696.
(7) Yang, Y.; Zhang, B. S.; Xu, W. D.; Shi, Y. B.; Jiang, Z. S.; Zhou, N. S.; Gu, B. X.; Lu, H. X. *J. Magn. Magn. Mater.* **2003**, *256*, 129.
(8) Gui, X. C.; Ye, W.; Wei, J. Q.; Wang, K. L.; Lv, R. T.; Zhu, H. W.; Kang, F. Y.; Gu, J. L.; Wu, D. H. *J. Phys. D: Appl. Phys.* **2009**, *42*, 075002.
(9) Song, W. L.; Cao, M. S.; Hou, Z. L.; Fang, X. Y.; Shi, X. L.; Yuan, J. *Appl. Phys. Lett.* **2009**, *94*, 233110.
(10) Zhang, X. G.; Liu, Y.; Qin, J. G. *Carbon* **2004**, *42*, 888.
(11) Narayanan, T. N.; Sunny, V.; Shaijumon, M. M.; Ajayan, P. M.; Anantharaman, M. R. *Electrochem. Solid-State Lett.* **2009**, *12*, K21.
(12) Liu, J. R.; Itoh, M.; Horikawa, T.; Machida, K.; Sugimoto, S.; Maeda, T. *J. Appl. Phys.* **2005**, *98*, 054305.
(13) Che, R. C.; Zhi, C. Y.; Liang, C. Y.; Zhou, X. G. *Appl. Phys. Lett.* **2006**, *88*, 033105.
(14) Zheng, Z.; Xu, B.; Huang, L.; He, L.; Ni, X. M. *Solid State Sci.* **2008**, *10*, 316.
(15) Zhao, D. L.; Li, X.; Shen, Z. M. *J. Alloys Compd.* **2009**, *471*, 457.
(16) Wang, C.; Lv, R. T.; Kang, F. Y.; Gu, J. L.; Gui, X. C.; Wu, D. H. *J. Magn. Magn. Mater.* **2009**, *321*, 1924.
(17) Tang, X.; Tian, Q.; Zhao, B. Y.; Hu, K. *Mater. Sci. Eng., A* **2007**, *445−446*, 135.
(18) Chen, Y. J.; Gao, P.; Wang, R. X.; Zhu, C. L.; Wang, L. J.; Cao, M. S.; Jin, H. B. *J. Phys. Chem. C* **2009**, *113*, 10061.
(19) Stein, A.; Wang, Z. Y.; Fierke, M. A. *Adv. Mater.* **2009**, *21*, 265.
(20) Wang, J. C.; Xiang, C. S.; Liu, Q.; Pan, Y. B.; Guo, J. K. *Adv. Funct. Mater.* **2008**, *18*, 2995.
(21) Liu, R. L.; Shi, Y. F.; Wan, Y.; Meng, Y.; Zhang, F. Q.; Gu, D.; Chen, Z. X.; Tu, B.; Zhao, D. Y. *J. Am. Chem. Soc.* **2006**, *128*, 11652.
(22) Zhou, J. H.; He, J. P.; Wang, T.; Sun, D.; Zhao, G. W.; Chen, X.; Wang, D. J.; Di, Z. Y. *J. Mater. Chem.* **2008**, *18*, 5776.
(23) Gao, P.; Wang, A. Q.; Wang, X. D.; Zhang, T. *Chem. Mater.* **2008**, *20*, 1881.
(24) Yao, J. Y.; Li, L. X.; Song, H. H.; Liu, C. Y.; Chen, X. H. *Carbon* **2009**, *47*, 436.
(25) Zhai, Y. P.; Dou, Y. Q.; Liu, X. X.; Tu, B.; Zhao, D. Y. *J. Mater. Chem.* **2009**, *19*, 3292.
(26) Wang, T.; Zhou, J. H.; Wang, D. J.; Sun, D.; Di, Z. Y.; He, J. P. *Acta Phys.−Chim. Sin.* **2009**, *25*, 2155.
(27) Sadaki, S.; Nakamura, K.; Hamabe, Y.; Kurahashi, E.; Hiroi, T. *Nature* **2001**, *410*, 555.

(28) Liu, R. L.; Ren, Y. J.; Shi, Y. F.; Zhang, F.; Zhang, L. J.; Tu, B.; Zhao, D. Y. *Chem. Mater.* **2008**, *20*, 1140.
(29) Park, I. S.; Choi, M.; Kim, T. W.; Ryoo, R. *J. Mater. Chem.* **2006**, *19*, 3409.
(30) Yu, T.; Deng, Y. H.; Wang, L.; Liu, R. L.; Zhang, L. J.; Tu, B.; Zhao, D. Y. *Adv. Mater.* **2007**, *19*, 2301.
(31) Ji, Z. H.; Liang, S. G.; Jiang, Y. B.; Li, H.; Liu, Z. M.; Zhao, T. *Carbon* **2009**, *47*, 2194.
(32) Yusoff, A. N.; Abdullah, M. H.; Ahmad, S. H.; Jusoh, S. F.; Mansor, A. A.; Hamid, S. A. A. *J. Appl. Phys.* **2002**, *92*, 876.
(33) Hong, Y. K.; Lee, C. Y.; Jeong, C. K.; Lee, D. E.; Kim, K.; Joo, J. *Rev. Sci. Instrum.* **2003**, *74*, 1098.
(34) Liu, Q. L.; Zhang, D.; Fan, T. X. *Appl. Phys. Lett.* **2008**, *93*, 013110.
(35) Liu, X. G.; Geng, D. Y.; Zhang, Z. D. *Appl. Phys. Lett.* **2008**, *92*, 243110.
(36) Zhang, X. F.; Dong, X. L.; Huang, H.; Lv, B.; Lei, J. P.; Choi, C. J. *J. Phys. D: Appl. Phys.* **2007**, *40*, 5383.
(37) Liu, X. G.; Geng, D. Y.; Meng, H.; Shang, P. J.; Zhang, Z. D. *Appl. Phys. Lett.* **2008**, *92*, 173117.
(38) Gorkunov, E. S.; Zakharov, V. A.; Ulyanov, A. I.; Chulkina, A. A. *Russ. J. Nondestruct. Test.* **2001**, *37*, 186.
(39) Shi, X. L.; Cao, M. S.; Yuan, J.; Fang, X. Y. *Appl. Phys. Lett.* **2009**, *95*, 163108.
(40) Deng, L. J.; Han, M. G. *Appl. Phys. Lett.* **2007**, *91*, 023119.
(41) Wang, C.; Han, X. J.; Xu, P.; Wang, J. Y.; Du, Y. C.; Wang, X. H. *J. Phys. Chem. C* **2010**, *114*, 3196.
(42) Chiu, S. C.; Yu, H. C.; Li, Y. Y. *J. Phys. Chem. C* **2010**, *114*, 1947.
(43) Liu, Z. F.; Bai, G.; Huang, Y.; Li, F. F.; Ma, Y. F.; Guo, T. Y.; He, X. B.; Lin, X.; Gao, H. J.; Chen, Y. S. *J. Phys. Chem. C* **2007**, *111*, 13696.
(44) Michielssen, E.; Sajer, J.; Ranjithan, S.; Mittra, R. *IEEE Trans. Microwave Theory Tech.* **1993**, *41*, 1024.
(45) Liu, Q. L.; Zhang, D.; Fan, T. X.; Gu, J. J.; Miyamoto, Y.; Chen, Z. X. *Carbon* **2008**, *46*, 461.
(46) Yu, B.; Qi, L.; Ye, J. Z.; Sui, H. *J. Appl. Polym. Sci.* **2007**, *104*, 2180.

JP911030N